ACS OMEGA

http://pubs.acs.org/journal/acsodf

Mini-Review

Recent Advances in Fluorescent Probes for Detection of HOCl and HNO

Anila Hoskere Ashoka, Firoj Ali, Rajeshwari Tiwari, Rina Kumari, Sumit Kumar Pramanik,* and Amitava Das*

Cite This: *ACS Omega* 2020, 5, 1730−1742

Read Online

ACCESS | Metrics & More | Article Recommendations

ABSTRACT: It is known that reactive oxygen (ROS) and nitrogen (RNS) species play a diverse role in various biological processes, such as inflammation, signal transduction, and neurodegenerative injury, apart from causing various diseases caused by oxidative and nitrosative stresses, respectively, by ROS and RNS. Thus, it is very important to quantify the concentration level of ROS and RNS in live cells, tissues, and organisms. Various small-molecule-based fluorescent/chemodosimetric probes are reported to quantify and map the effective distribution of ROS/RNS under in vitro/in vivo conditions with a great spatial and temporal resolution. Such reagents are now appreciated as an excellent tool for aiding breakthroughs in modern redox biology. This mini-review is a brief, but all-inclusive, account of such molecular probes that have been developed recently.

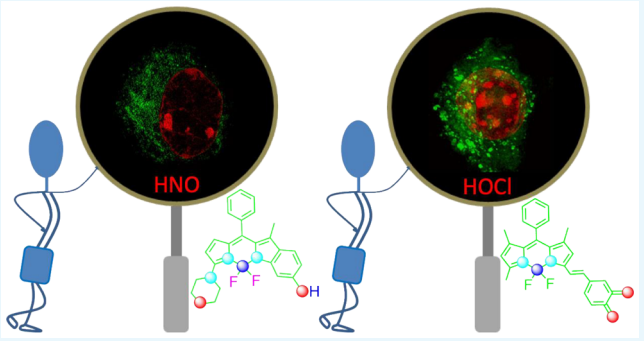

INTRODUCTION

In recent years, the efficacies of clinical diagnostics, therapeutics, and medicines have emerged due to our better insights and recent advances in the understanding of various biological processes at the cellular and molecular levels.[1] The biology of reactive oxygen and nitrogen species (ROS and RNS, respectively) is linked to the involvement of these intracellular molecular entities in various biological processes.[1−3] Endogenous ROS and RNS are formed through various intracellular biochemical processes, including nicotinamide adenine dinucleotide phosphate oxidase and mitochondrial electron transport chain.[4,5] Exogenous sources (e.g., radiation, air pollutants, and certain redox-active xenobiotics) also cause an elevated level of ROS/RNS in living organisms.[6] ROS/RNS participate in biological processes as immunotoxins as well as immunomodulators, and their effective build-up in a living organism is linked to its generation as the byproducts of aerobic metabolism and the immune system processes.[7] Accumulation of the higher than the optimal level of ROS overhauls the antioxidant mechanisms and attributes to oxidative cellular stress.[8] Mechanisms or the biochemical processes which control the production of intracellular ROS/RNS are not well comprehended, and it is pertinent to develop diagnostic strategies at cellular sites of dysfunction.[9]

Among various ROS and RNS that are operational in living organisms, we shall limit our discussions on the strategies for clinical diagnosis of hypochlorous acid (HOCl) as ROS and nitroxyl (HNO) as the RNS for this mini-review. The biochemistry of HOCl helps the neutrophils to kill a wide range of infectious agents.[10] It is produced during an oxidation reaction between the H_2O_2 and Cl^- ions which is catalyzed by the myeloperoxidase (MPO) enzyme, excreted by neutrophils in its inflammatory state.[10] Even though it plays a defensive role in human health, the elevated levels of HOCl are known to cause tissue damage and several diseases such as obesity, diabetes, atherosclerosis, lung injury, rheumatoid, cardiovascular diseases, neurodegenerative conditions, and various cancers.[10,11]

The chemistry of HNO (nitroxyl) and its conjugated base NO^- is rather less explored as compared to HOCl. HNO is the protonated one-electron reduction product of NO and is isoelectronic with an oxygen molecule (O_2). Unlike HOCl, the knowledge base for insight into the role of HNO in human physiology is still in its infancy. Angeli's salt is the most commonly used chemical for the in situ generations of HNO (rate constant of 4.6×10^{-4} s^{-1} (at room temperature)), and this process is favored over a pH range of 4−8.[12,13] Commercial availability of this salt has helped in developing the mechanistic insights of reactions involving HNO with a particular emphasis

Received: October 14, 2019
Accepted: December 24, 2019
Published: January 21, 2020

https://dx.doi.org/10.1021/acsomega.9b03420
ACS Omega 2020, 5, 1730−1742

on elucidation of the biochemical/physiological role. The linear HNO structure is less stable than the bent form by ca. 67 kcal/mol. Computational studies predicted the possible presence of a triplet state having energy of 18.0−19.0 kcal over the ground singlet state.[14,15] However, to date, experimental evidence for ^{3}HNO is missing. Importantly, for NO^- the triplet state (ground state) is more stable than the singlet state by ca. 16 kcal/mol.[16] Thus, the deprotonation process is associated with a change in spin state and is spin forbidden (adiabatic singlet−triplet transition energy is 18.45 kcal/mol),[17] and its generation is a slow process, which is attributed to HNO as the prevalent species (pK_a^{HNO} = 11.4)[18] at physiological pH.

HNO is associated with numerous biological activities with significant therapeutic potential. A series of reports reveal that the alcohol-deterrent drug cyanamide (NH_2CN) is really a prodrug for HNO, an inhibitor of the aldehyde dehydrogenase enzyme.[19] HNO has unique positive lusitropic and ionotropic effects in heart failure without a chronotropic effect and shows favorable effects in ischemia-reperfusion injury. Recent studies also reveal the role of HNO in cancer therapy.

Considering such significances, reagents for efficient recognition, quantification, and mapping of intracellular HOCl and HNO-inappropriate organelles or quantification in suitable biofluids are highly desired. This has attracted much attention among the researchers who are active in the area of chemical biology, environmental science, and clinical diagnostics. In recent years, a number of reports on fluorogenic receptors describing specific detection of these two analytes have appeared. In this short account, we shall limit our discussion only to the recently reported chemodosimetric receptors for HOCl and HNO. There is a recent account published by Wu, Chen, Yoon, and their co-workers on receptors that are specific toward HOCl. Those examples shall be avoided in this mini-review to avoid any repetition.

RESULTS AND DISCUSSION

Receptors for HOCl. HOCl is an efficient antimicrobial ROS with high oxidizing potential and is commonly produced in higher eukaryotes. HOCl oxidizes amino acids containing amines and sulfurs; in particular, methionine residues are oxidized to the corresponding methionine sulfoxide. The conversion of methionine sulfoxide is an efficient one with reaction rate approaching the diffusion limit. Recent studies reveal that a HOCl-specific transcription factor (HypT) contributes to HOCl resistance by upregulating the biochemical synthesis of three methionine residues (Met123, Met206, and Met230). This oxidizing efficiency of HOCl is being largely utilized for developing various chemodosimetric molecular probes.

Yang and his team reported an aqueous-soluble *p*-methoxyphenol derivative (**1**) as the dual-signaling (colorimetric and fluorimetric) chemodosimetric probe for HOCl in aqueous PBS buffer (pH 7.4) medium (Figure 1).[20] Following oxidation of **1** to the corresponding quinonoid derivative, a distinct change in the absorption maxima from 314 to 393 nm was observed with an associated reduction in the emission quantum yield at 388 nm. Other ROS and RNS species (H_2O_2, $^1O_2$, $O_2^{\bullet-}$, $^{\bullet}OH$, $^{\bullet}NO$, $ONOO^-$, and $ROO^{\bullet}$) failed to induce, and detectable changes in the optical spectrum for **1** and these data ensured specificity of this reagent toward HOCl. This was one of the initial reports on HOCl recognition. Presumably, the luminescence quenching process was the deterrent factor for the authors for exploring the option of using this reagent for intracellular studies.

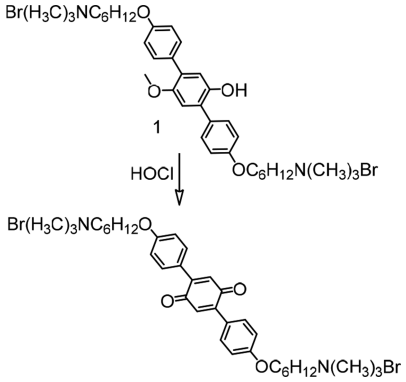

Figure 1. Recognition process for HOCl by the reagent **1**.

Chen et al. reported the iridium(III) complex (**2**) having an oximated 2,2′-bipyridine for detection of ClO^-.[21] A facile C═N−OH isomerization was attributed to an efficient nonradiative decay process and the poor emission quantum yield (Figure 2). Selective oxidation of the oxime to an aldehyde

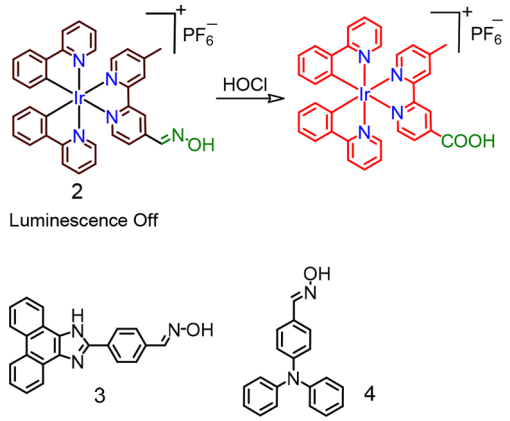

Figure 2. Molecular structures of chemosensors **2**−**4**.

or carboxylic acid, induced by ClO^-, caused a luminescence ON response having a luminescence maximum at 578 nm (λ_{ex} = 346 nm) in DMF:aq. HEPES buffer medium (pH 7.2). An oxidized carboxy derivative showed a bright orange-yellow luminescence coming from from [5d(Ir) → π^*(bpy)] ^{3}MLCT and [π(ppy) → π^*(bpy)] ^{3}LLCT triplet excited states. The authors ensured the specificity of the reagent **2** toward ClO^- in the presence of other common ROS species. Moreover, the use of test strips comprising **2** showed very promising sensitivity to ClO^-. Similar oxime based probes **3** and **4** were also reported for specific detection of ClO^-.[22,23]

A similar methodology was utilized for developing a rhodamine-based luminophore (**5**), and this was further explored for mapping of the endogenous HOCl in live HeLa cells (Figure 3).[24]

Loo, Zhang, and co-workers reported a hybrid upconversion luminescence (UCL) detection system (**6**) for HOCl (Figure 4).[25] Upconverting luminescence nanoparticles (UCNP) are generally preferred over conventional luminescent molecular probes owing to their stability toward photobleaching, deeper tissue penetration of the near-infrared (NIR) active radiation, minimal or no self-induced fluorescence, and less tissue damage.[26−28] The extent of loading of the rhodamine-based oxidizable receptor was calculated as ∼5.81 wt %. The amino-terminated rhodamine derivative was

https://dx.doi.org/10.1021/acsomega.9b03420
ACS Omega 2020, 5, 1730−1742

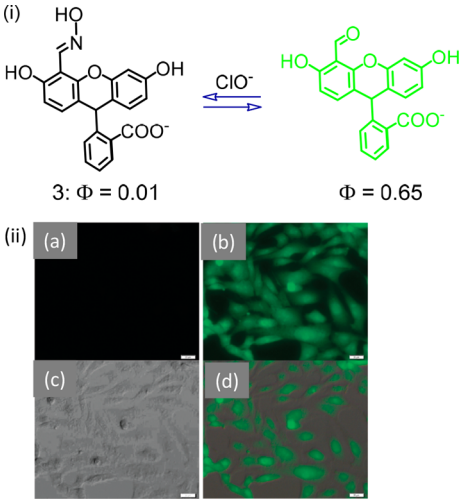

Figure 3. (i) Molecular structure for reagent **5** and (ii) fluorescence and bright-field microscopy images of cells. (a) Fluorescence microscopy image of cells incubated with **5** (20 μM) for 30 min. (b) Fluorescence microscopy image of cells pretreated with **5** (20 μM) for 30 min and then incubated with OCl (200 μM) for 30 min. (c) Bright-field microscopy image of the cells shown in panel b. (d) Overlay image of (b) and (c). Figure 3(ii) was reprinted from ref 24. Copyright 2011 Royal Society of Chemistry.

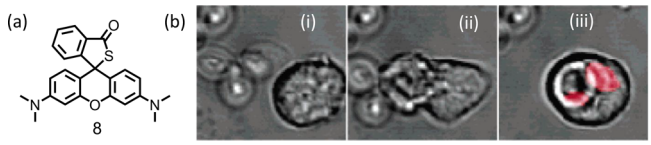

Figure 5. (a) Molecular structure of **8** and (b) CLSM images of porcine neutrophil: (i) zymosan particles are near the neutrophil, (ii) the neutrophil engulfs the zymosan, and (iii) phagocytosis is complete. The Figure 5b was reprinted from ref 30. Copyright 2007 American Chemical Society.

loaded onto the surface of UCNPs via interactions with oleic acid (OA) termini. Polyacrylic acid (PAA) was further used to replace OA ligands from the surface of UCNPs, which not only helped in creating an aqueous-soluble triple-layer nanostructure but also prevented the rhodamine derivative from detachment from the UCNP surface. Upon reaction of **6** with HOCl, there was a gradual decrease in green emission from UCL with concomitant increase in the rhodamine-based emission due to the conversion of the cyclic lactam from an acyclic xanthene form through an efficient FRET-based energy transfer process. This ratiometric response was successfully utilized for mapping intracellular HOCl that was released by MPO-mediated peroxidation of chloride ions in living cells. A similar probe **7** was further reported by Xu et al. for specific detection of HOCl.[29]

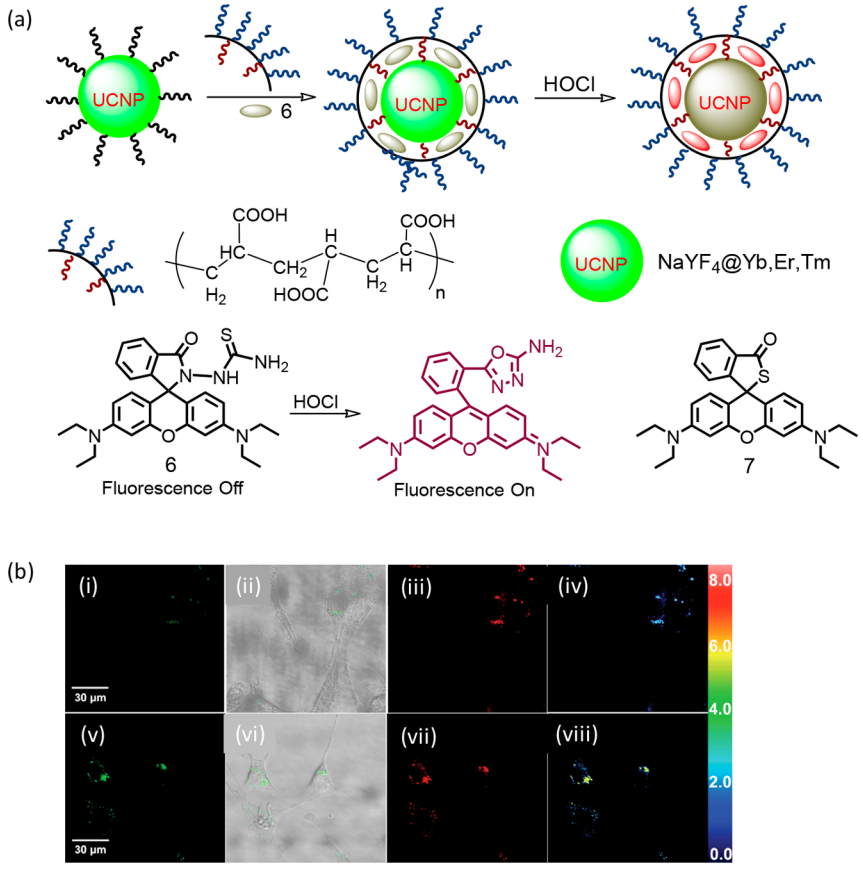

Figure 4. (a) Schematic representation of the hybrid UCNP-based recognition of HOCl and the molecular structures for **6** and **7**. (b) Ratiometric UCL images of NIH3T3 cells: the cells preincubated with hybrid-UCNPs in the MPO enzymatic system (MPO enzyme, 2.0 U/100 mL; NaCl, 250 mM) for 30 min at 37 °C and then further incubated with 100 μM H_2O_2 for 180 min (i–iv). Emissions were collected by the green UCL window at $\lambda_{500-560}$ nm (i and v) and red UCL window at $\lambda_{600-700}$ nm (iii and vii) with excitation at 980 nm. Overlay of bright-field and green channel UCL images shown in the panel (ii and vi). The ratiometric UCL intensities of NIH3T3 cells (iv and viii) were examined by using IPP software. Figure 4b was reprinted from ref 25. Copyright 2014 John Wiley and Sons.

https://dx.doi.org/10.1021/acsomega.9b03420
ACS Omega 2020, 5, 1730−1742

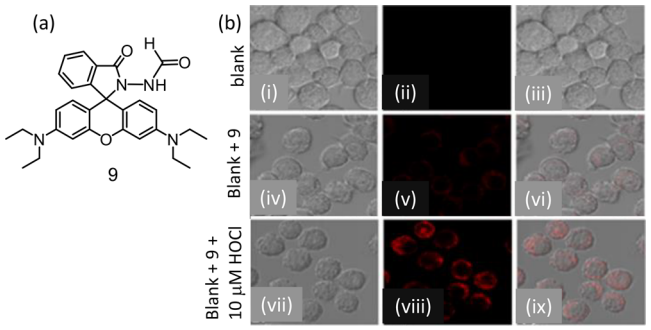

Figure 6. (a) Molecular structure of reagent **9** and (b) fluorescence microscopy images of live RAW 264.7 macrophage cells: (i, iv, and vii) are bright-field images; (ii, v, and viii) are of red channel at 570−670 nm) with excitation at 533 nm; and (iii, vi, and ix) are the merged images. Figure 6b was reprinted from ref 31. Copyright 2019 American Chemical Society.

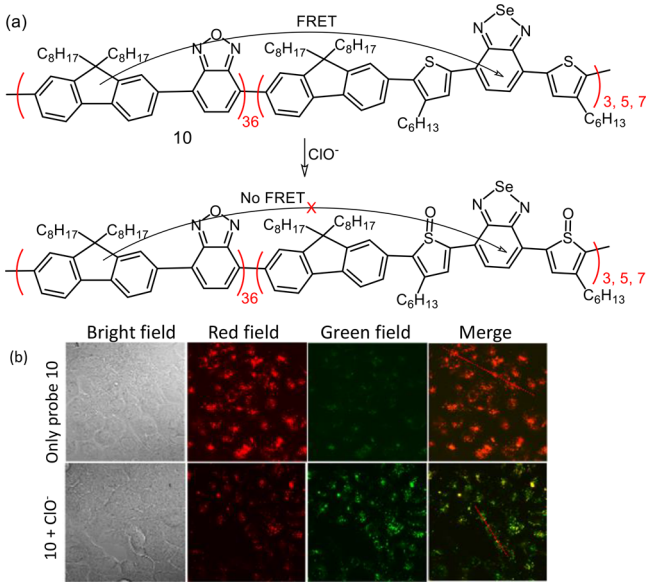

Figure 7. (a) Schematic presentation of the chemodosimetric detection of ClO^- and (b) CLSM images of exogenous ClO^- in MCF-7 cells: MCF-7 cells were first incubated with **10** (10 μg/mL) overnight at 37 °C and then were incubated with 80 μM NaClO. CLSM images were acquired in the green channel (530−600 nm) and red channel (>650 nm) with λ_{ex} = 405 nm. Figure 7b was reprinted from ref 32. Copyright 2017 American Chemical Society.

The sulfur-containing rhodamine derivatives showed greater selectivities for OCl^- than those of Se and Te. In 2007, Nagano and co-workers presumably were the first to demonstrate this using an appropriate S-functionalized rhodamine derivative (**8**).[30] Authors have also demonstrated the use of this reagent for mapping the hypochlorous acid that was created inside phagosomes in real time (Figure 5).

The authors have reported a formylhydrazine derivative of rhodamine B (**9**) for specific recognition of intracellular HOCl in live RAW 264.7 macrophage cells (Figure 6).[31]

A single conjugated flexible polymer having reactive centers for HOCl and target-inert fluorophores was designed. This far-red to NIR nanoprobe (**10**) helped in identifying intracellular HOCl through a FRET-based ratiometric detection (Figure 7).[32] Reagent **10** was successfully used for mapping of HOCl fluctuations in macrophage cells. The dual-emission property of **10** enabled a more sensitive mapping of ClO^- in peritonitis in mice with high contrast.

The azo functionality having an *o*-amino group substituted in a phenyl ring undergoes selective oxidation with HOCl to produce a triazole functionality. This was utilized in developing Ru(II)-polypyridyl-based luminescent sensors (**11** and **12**) for HOCl (Figure 8).[33]

BODIPY derivative (**13**, Figure 9) was used successfully for mapping endogenously produced HOCl in RAW 264.7 macrophages.[34] Wide-field and super-resolution structured illumination microscopy (SR-SIM) images confirmed localization of the reagent in the Golgi complex and lysosomes. Importantly, reagent **13** was found to be suitable with 3D-SIM imaging of a single cell.

Two-Photon Reagents for HOCl Recognition. Presumably, the first two-photon (TP) active reagent for HOCl was reported by Chang and co-workers.[35] The first TP-active reagents (**14** and **15**) that were specific for imaging HOCl in the mitochondria (**14**) and lysosome (**15**) are shown in Figure 10.[35] These probes showed good selectivity toward HOCl. In particular, the TP imaging of **14** and **15** in the murine model revealed that the elevated amount of HOCl could be identified in both the mitochondria and lysosome of macrophage cells under inflammation conditions. Thus, these reagents could be utilized to understand the roles of HOCl at subcellular levels.

A new TP fluorescent probe (**16**) having a pendant imidazoline-2-thione as an OCl^- identification unit and triphenylphosphine as a mitochondrial-targeting group were reported.[36] The precise reaction among imidazoline-2-thione and OCl^- accounted for the luminescence ON response and the basis for specific recognition even in the presence of other ROS species. This TP-active reagent **16** was utilized to image endogenously created mitochondrial OCl^- in live HeLa, HepG2, and RAW 264.7 cells

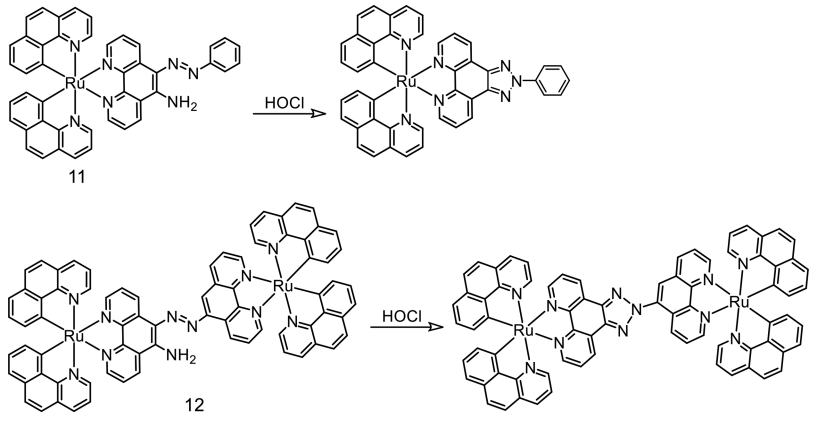

Figure 8. Molecular structures of probes **11** and **12**. The proposed mechanism of the probe toward hypochlorous acid.

https://dx.doi.org/10.1021/acsomega.9b03420
ACS Omega 2020, 5, 1730−1742

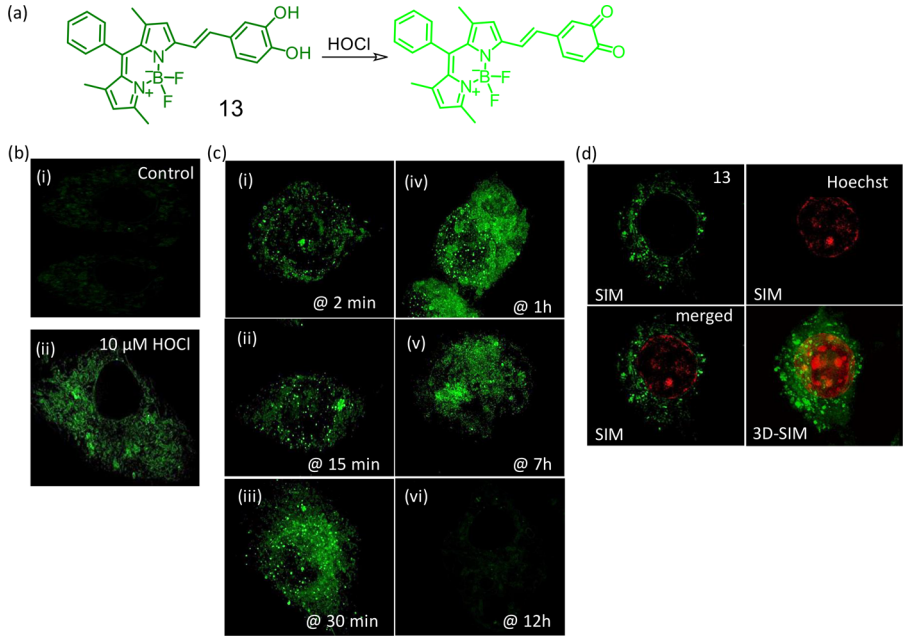

Figure 9. (a) Schematic presentation of the chemodosimetric detection of ClO^- by the reagent **13**. (b) SR-SIM images of RAW 264.7 cells (i) incubated with **13** as control for 30 min, (ii) incubated with **13** and further exposed to 10 μM HOCl for 20 min. (c) 3D-SIM images of endogenously generated HOCl and reduced signal spread generated by lipopolysaccharide stimulation (2500 ng) detected by **13** (10 μM). (i and ii) Signal detection on punctured structures, (ii–iv) signal spread from punctures to diffuse structures, (v) shows more diffuse structures than punctures signifying total signal transfer to diffuse structures from punctures, and (vi) signal saturation due to less accessibility of endogenous HOCl (indication of cell death). (d) Dual-color SR-SIM and 3D-SIM using **13** in the presence of lipopolysaccharide and Hoechst 33442. Figure 9(b–d) was reprinted from ref 34. Copyright 2018 Royal Society of Chemistry.

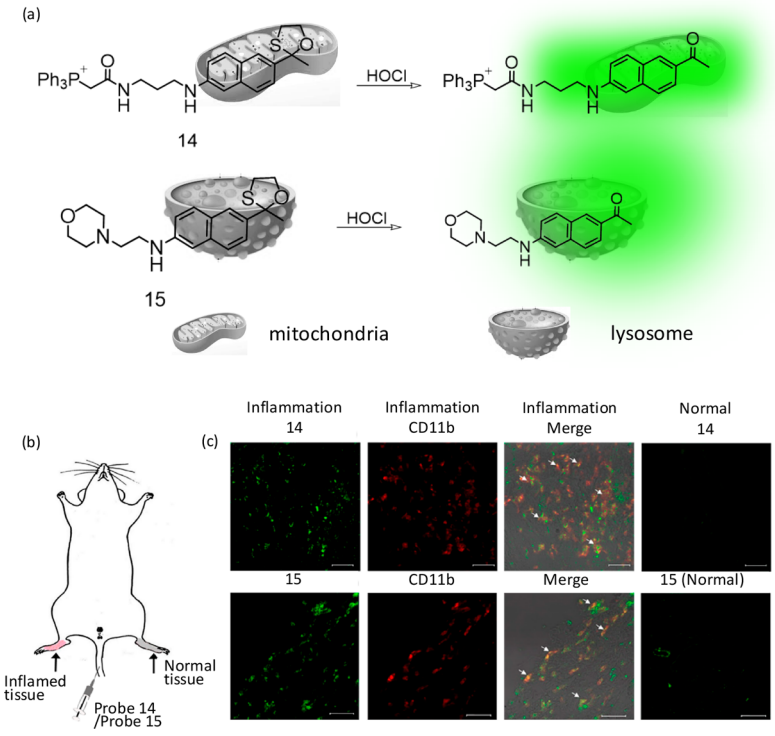

Figure 10. Molecular structure for receptors (a) **14** and **15** and (b) detection of lipopolysaccharide-dependent HOCl production in inflammation tissues via **14** and **15**. An amount of 200 μL of lipopolysaccharides (1 mg/mL) was hypodermically injected into the right rear paws of the mouse to cause inflammation. After 1 day, 200 μL of 1 mM **14** (or **15**) was intravenously injected, and the paw skin was sectioned 1 h later. (c) CLSM images of reagent and CD11b in the inflamed tissue. Reagent fluorescence, green; antibody CD11b, red. Arrows signify the merged parts of HOCl-sensitive probes and CD11b. Scale bar: 30 μm. Figure 10(b,c) was reprinted from ref 35. Copyright 2015 American Chemical Society.

via TP microscopy (Figure 11). Despite being TP-active, this reagent was not utilized for tissue imaging.

The two-photon activity of the naphthalimide derivative was utilized for developing a lysosome-specific luminescent

https://dx.doi.org/10.1021/acsomega.9b03420
ACS Omega 2020, 5, 1730–1742

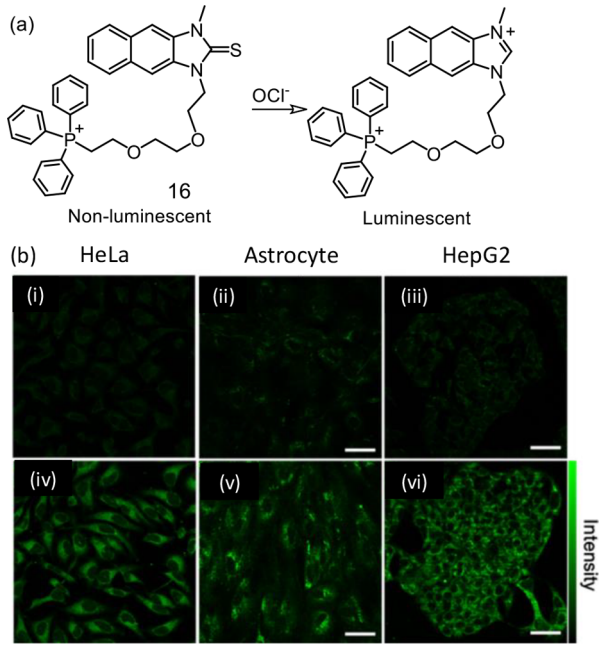

Figure 11. (a) Schematic presentation of the chemodosimetric detection of ClO^- by the reagent **16**. (b) TPM images of (i, iv) HeLa cells, (ii, v) astrocytes, and (iii, vi) HepG2 cells labeled with 10 μM **16** (i–iv) before and (iii–vi) after pretreatment with 200 μM NaOCl for 30 min. The TPM was collected at 400–600 nm upon excitation at 700 nm with femtosecond pulses. Scale bars: (upper) 48 μm and (lower) 18 μm. Figure 11b was reprinted from ref 36. Copyright 2017 American Chemical Society.

molecular probe (**17**) that had morpholine functionality as the lysosome-targeting group.[37] Reagent **17** was oxidized to the corresponding sulfoxide species by ClO^- with an associated luminescence OFF response. Unlike other examples, this reaction triggered an OFF response, which could be revived by GSH.

The naphthoimidazolium borane derivative (**18**) participated in an electrophilic oxidation mechanism associated with B–H bond degradation to yield a TP-active naphthoimidazolium derivative.[38] This reagent could be utilized for monitoring of endogenously produced HOCl and the changes in endoplasmic reticulum during oxidative stress situations. Endogenous OCl^- mapping in macrophages was then studied. Macrophages were stimulated by lipopolysaccharides (LPS) and interferon γ (IFN-γ). MPO was attributed to an in situ generation of OCl^- and was further treated with phorbol myristate acetate (PMA). These studies confirmed the efficacy of the reagent for recognition of intracellular OCl^- through TP microscopy (Figure 12).

Guo and co-workers have reported a series of reagents for intracellular quantification of HOCl by introducing a bioorthogonal dimethylthiocarbamate receptor (Figure 13).[39] The authors have successfully demonstrated the role of the S atom in designing this set of molecular probes (Figure 13 a). Among these, reagent **19** is found to be the most efficient one, while allowing a ratiometric luminescence response on a specific reaction with HOCl at high risk pathogenic concentrations (0.47 mM). This reagent showed 48-fold enhancement in the ratio for $I_{468\ nm}/I_{630\ nm}$ with a good linear relationship. The release of the thiocarbamate moiety of **19** on reaction with HOCl led to the generation of the corresponding phenol derivative having a luminescence maximum of 468 nm. The

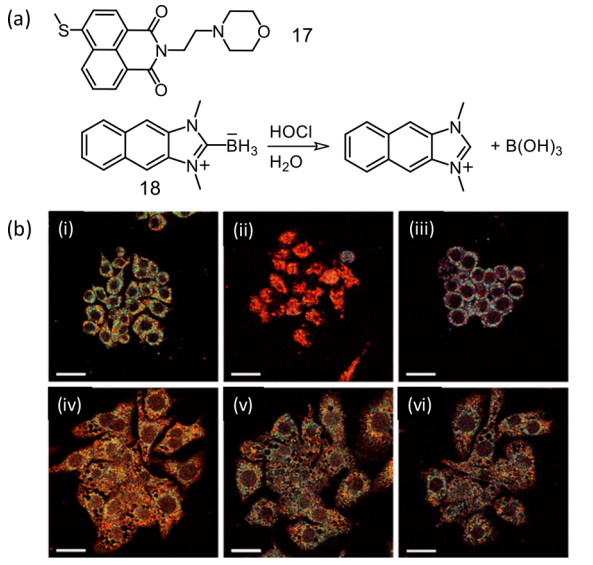

Figure 12. (a) Molecular structures for reagents **17** and **18**. (b) Pseudocolored ratiometric TPM images of Raw 264.7 cells labeled with **18** (10 μM) for 30 min: (i) control image. Cells pretreated with (ii) tunicamycin (known to increase oxidative stress of the ER (10 μg mL^{-1}, 16 h)) through generation of H_2O_2, (iii) dithiothreitol that consumes H_2O_2 in the ER and reduces oxidative stress (2 mM, 16 h), (iv) lipopolysaccharides (100 ng mL^{-1}, 16 h), interferon-γ (50 ng mL^{-1}, 4 h), and phorbol myristate acetate (10 nM, 30 min), (v) lipopolysaccharides, interferon-γ, phorbol myristate acetate, and 4-aminobenzoic acid hydrazide (a MPO inhibitors) (50 μM, 4 h), and (vi) lipopolysaccharides, interferon-γ, PMA, and FFA (50 μM, 4 h) and then treated with **18** (λ_{ex} = 720 nm), and TP microscopy images were acquired at 450–600 nm (green) and 380–430 nm (blue) channels. The scale bar is 20 μm. Figure 12b was reprinted from ref 38. Copyright 2017 American Chemical Society.

formation of the phenolic derivative induced an excited-state intramolecular proton transfer and intramolecular charge transfer processes to result in a 468 nm luminescence. The authors could demonstrate the use of this reagent for monitoring the oxidative stress process induced by elesclomol in live cancer cells (Figure 13b).

VARIOUS RECEPTORS FOR HNO

Initially it was perceived that HNO chemical biology was similar to NO as a biological conciliator. Unfavorable redox potential does not allow a facile reduction of NO to HNO in physiological conditions. However, moderate H–NO bond strength (50 kcal mol^{-1}) makes HNO a more efficient hydrogen atom donor than many other biological antioxidants. This may potentially react with the appropriate ROS/RNS-based radical species to generate NO, which subsequently reacts, oxidizing radical species to quench.[40] There is a recent short account on receptors that are specific toward HNO published by Lin and co-workers. We shall be avowing any appreciable overlap with examples that are discussed in this mini-review.

Thus, the reactivity and biological implications of HNO and NO are not similar; it is worth knowing some of the early reports by Lippard and co-workers in NO recognition. These results have certainly helped researchers in understanding the clinical biology of HNO and are mentioned briefly before discussing some of the recent efforts on HNO recognition.

Lippard's group reported a series of Cu(II) complexes for the detection of NO and were almost silent toward HNO. One of

https://dx.doi.org/10.1021/acsomega.9b03420
ACS Omega 2020, 5, 1730–1742

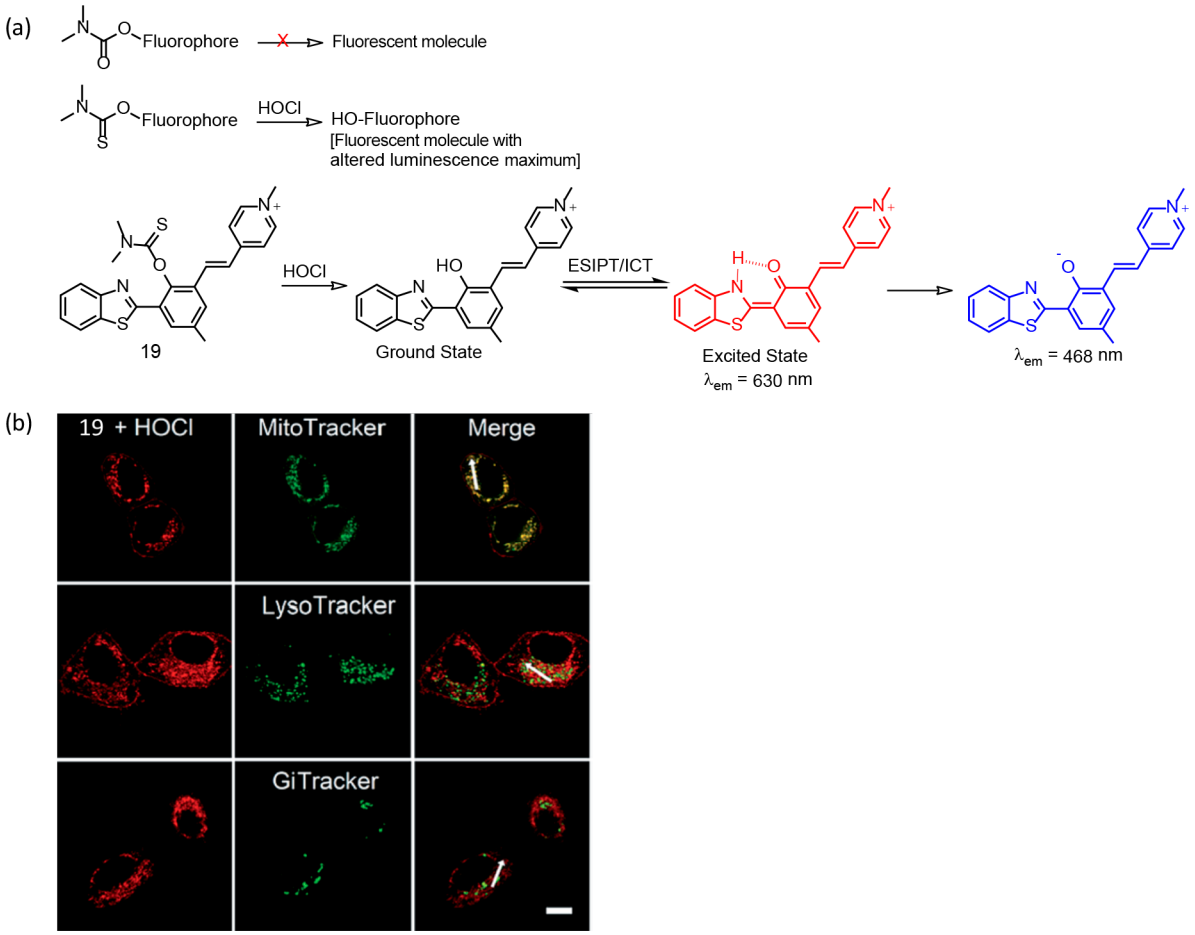

Figure 13. (a) Scheme for demonstrating the role of the S atom in the chemodosimetric recognition process and the molecular structure for reagent **19** with illustration of the photoinduced processes that are associated with the ratiometric luminescence response. (b) Intracellular localization of **19** in HepG2 cells: CLSM imaging of HepG2 cells incubated with 20 mM **19** and then stained with MitoTracker Green FM (200 nM), LysoTracker Green DND-26 (7.5 nM), and Golgi Tracker Green (NBD C6-ceramide, 3 mM), respectively. Red channel: λ_{ex} = 405 nm, λ_{em} = 610−650 nm. Green channel: λ_{ex} = 488 nm, λ_{em} = 490−550 nm. The scale bar is 10 mm. Figure 13b was reprinted from ref 39. Copyright 2019 Royal Society of Chemistry.

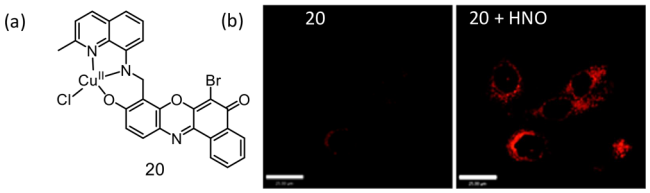

Figure 14. (a) Molecular structures of probe **20**. (b) CLSM imaging of HNO in HeLa cells. The left image corresponds to the treatment of cells with the reagent **20**. The right side image corresponds to cells treated with Angeli's salt. Scale bar = 25 μm. Figure 14b was reprinted from ref 41. Copyright 2013 American Chemical Society.

the representative Cu(II) complexes (**20**) is shown in Figure 14. These probes were successfully imaged NO in HeLa cells and RAW 264.7 macrophages.[41] Luminescence response of **20** toward NO was specific. Experimental studies revealed that the NO-triggered fluorescence enhancement for 19 happened through generation of Cu(I) with subsequent dissociation to a luminescent secondary amine N−NO derivative.

To explicate the factors that impart the selectivity for nitroxyl (HNO) over nitric oxide (NO) among the metal-based fluorescent reagents, Lippard and co-workers had studied a series of Cu(II)-cyclam derivatives, and the one (**21**) that showed most positive reduction potential of the series promoted reduction of Cu(II) (Figure 15).[42] Generation of Cu(I) with necessary

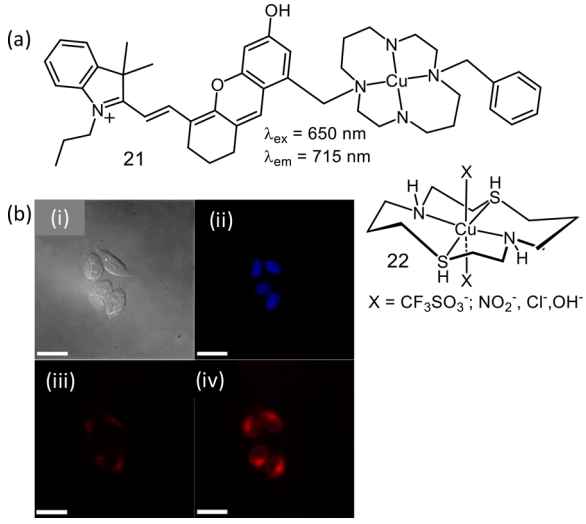

Figure 15. (a) Molecular structure of probes **21** and **22**. (b) CLSM images of HeLa cells incubated with **21** in aq. PBS buffer solution before and after addition of Angeli's salt: (i) differential interference contrast image, (ii) blue channel image showing nucleus, (iii) NIR channel prior to the addition of Angeli's salt, and (iv) NIR channel 5 min after treatment with 1.5 mM Angeli's salt. The scale bar is 25 μm. Figure 15b was reprinted from ref 42. Copyright 2014 American Chemical Society.

https://dx.doi.org/10.1021/acsomega.9b03420
ACS Omega 2020, 5, 1730−1742

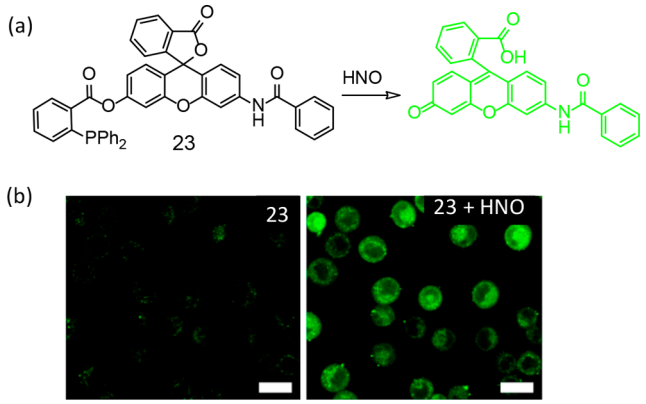

Figure 16. (a) Molecular structure of probe **23**. (b) HNO-induced CLSM images of A549 cells stained with 1 μM **23** before (left) and 15 min (right) after treatment with 2 μL of Angeli's salt in 10 mM aq. NaOH solution (200 μM). Scale bar = 20 μm. Figure 16b was reprinted from ref 44. Copyright 2013 American Chemical Society.

structural changes to adjust and stabilize the tetrahedral Cu(I) center was stated to be crucial and attributed to a luminescence ON response. It is worth mentioning that reduction of the nitrosonium cation (NO^+) to NO occurs at 1.52 V (vs NHE) and fails to reduce Cu(II) in **21**. This is attributed to the specificity toward HNO over NO. Lippard and co-workers have developed another Cu(II) complex (**22**) of the mixed thia/aza 14-N_2S_2 ligand, which was found to react reversibly with HNO at pH 7.[43]

Nakagawa et al. introduced a rhodamine-based HNO specific probe **23** utilizing diphenylphosphine as a response site. HNO reacted with the probe to yield a luminescent rhodamine derivative (Figure 16).[44]

An analogous methodology was utilized by Lin et al. for developing reagents (**24**–**26**) that were sensitive to HNO and showed turn ON luminescence response.[45] Diphenylphosphine as a responsive site was exploited for designing these receptors. The reagents could show various emission colors from green to NIR in response to HNO in aqueous solution and inside the cells (Figure 17). For the first time, by incubating the living cells with these reagents simultaneously, we demonstrate the multicolor imaging of HNO with emission colors in the range of green to NIR in living systems. Furthermore, reagent **27** showed large turn-on NIR fluorescence signal upon excitation in the NIR region. This reagent was also used successfully for detection of HNO in living mice. The same research group has exploited a similar approach for developing another rhodamine derivative for recognition of intracellular HNO.[46]

A similar reaction was utilized by Das and co-workers for developing another reagent **28**.[47] This reagent showed high specificity toward HNO and localization at the endoplasmic reticulum of RAW 264.7 cells. This photophysical property of this reagent was found to be well-suited for its use in SR-SIM and two-color SIM imaging, permitting more than one organelle to be imaged at SR-SIM (Figure 18). The option of using this probe for in vivo imaging application was exhibited using a small marine invertebrate model, Artemia. Designed substitution at the pyrrole ring with extended conjugation helped in achieving a luminescence response with maximum at longer wavelength (586 nm).

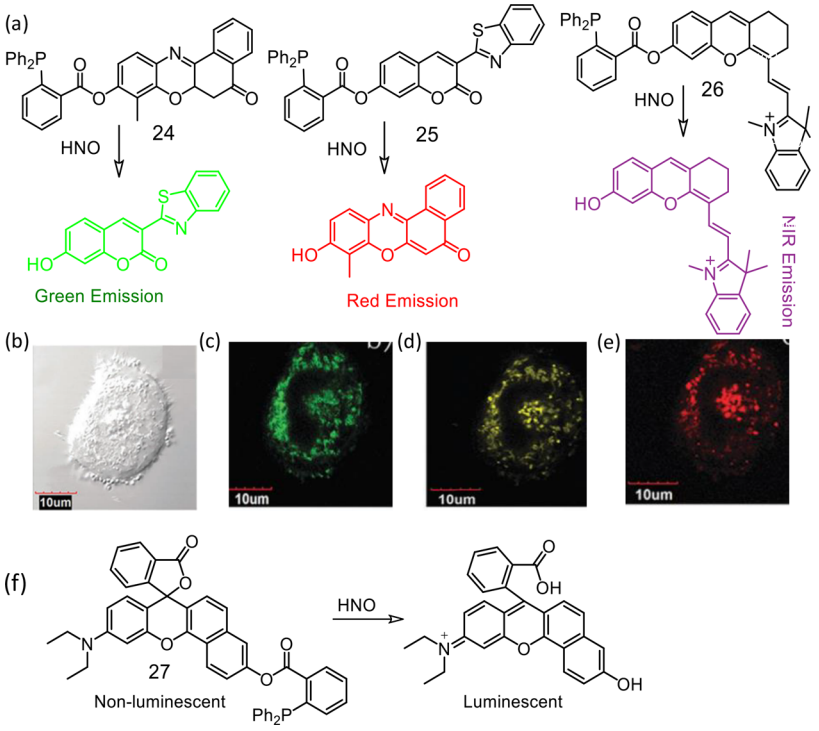

Figure 17. (a) Chemical structures of the molecular probes **24**–**26**. CLSM images of living HeLa cells: (b) bright-field image of live HeLa cells after incubation with **24** (5.0 μM), **25** (10 μM), and **26** (5.0 μM) for 20 min, then with Angeli's salt (200 μM) for 45 min; (c) CLSM image of (b), λ_{ex} = 405 nm, emission channel of 470–570 nm; (d) CLSM image of (b), λ_{ex} = 559 nm, emission channel of 600–680 nm; (e) CLSM image of (b), λ_{ex} = 635 nm, emission channel of 690–780 nm. The scale bar is 10 μm. (f) The chemical structure of the probe **26** and its chemodosimetric reaction. Figure 17(b–e) was reprinted from ref 45. Copyright 2016 Royal Society of Chemistry.

https://dx.doi.org/10.1021/acsomega.9b03420
ACS Omega 2020, 5, 1730–1742

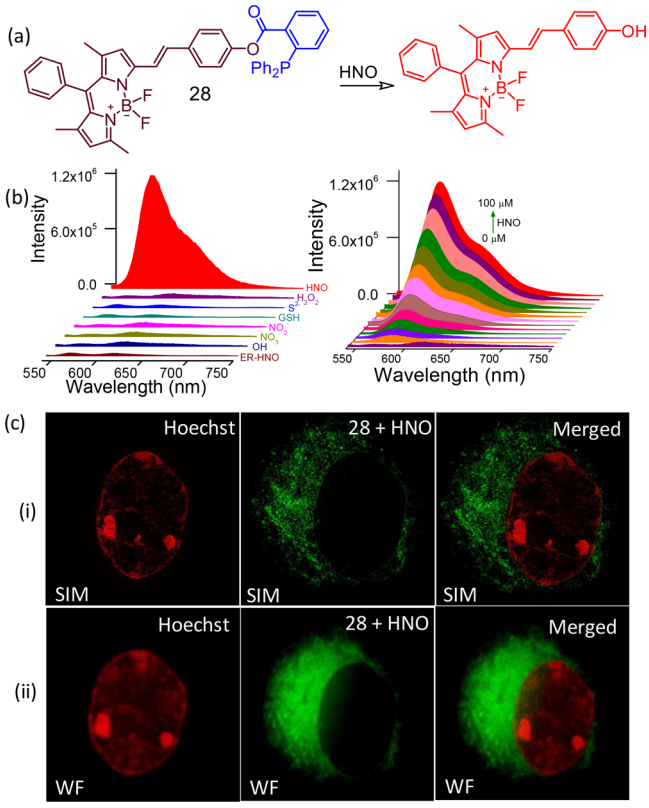

Figure 18. (a) Molecular structure of the reagent **28**, (b) luminescence spectral profile to show the specificity of the reagent toward **28** and its concentration-dependent intensity variation, (c) dual-color (i) SIM and (ii) comparative wide-field CLSM images with Hoechst as the nuclear stain (pseudo coloring has been employed in all the images) and **28** as the ER-specific stain. Figure 18(b,c) was reprinted from ref 47. Copyright 2017. American Chemical Society.

The analogous methodology was adopted for developing another new BODIPY derivative (**29**) for specific recognition of HNO.[48] The hydrophobic interior of an amphiphilic copolymer (mPEG-DSPE; DSPE: 1,2-dimyristoyl-*sn*-glycero-3-phosphoethanolamine-*N*-(methoxy(polyethylene glycol)-2000) was utilized for encapsulating the reagent **29** to prepare a micellar nanoprobe. This reagent showed a ratiometric luminescence response on specific reaction with HNO. Reagent **29** showed efficient cellular internalization and was effectively used to detect HNO in living HepG2 cells, as well as in zebrafish larvae (Figure 19).

As discussed earlier, the reactivity of HNO with biological thiols reaches the diffusion control limit with rate constants $\sim 10^9$ M^{-1} s^{-1}. To address this, Chan and co-workers had reported a new thiol-based reagent (**30**) that had the potential to compete against reactive thiols for HNO.[49] The molecular structure and the luminescent reaction product are shown in Figure 20. Treatment of **30** with an HNO donor resulted in a 16-fold enhancement in luminescence intensity. Authors have argued that this reagent showed improved specificity over various ROS/RNS species and efficacy in the presence of biothiols (e.g., glutathione in mM concentrations).

CONCLUSIONS

Significant advances are achieved in designing appropriate receptors for HOCl and HNO, and some of the initial and most recent examples are summarized in this short account. However, more concerted efforts are still needed to design the probe for efficient application in clinical biology and therapeutics. To date, there are only a few examples that are either NIR-active or TP-active. Such reagents open up the possibility of developing more efficient reagents. It is argued that one of the unanswered questions in the field of HNO pharmacology/physiology remains: is HNO endogenously generated as a physiological effector/mediator? A question which could, perhaps, be addressed by developing a reagent that tracks/maps the HNO generated through endogenous biosynthesis during cardiovascular stress. Researchers have not addressed the query: how can HNO discriminate between thiol proteins? Addressing such unanswered questions would help in developing an insight into

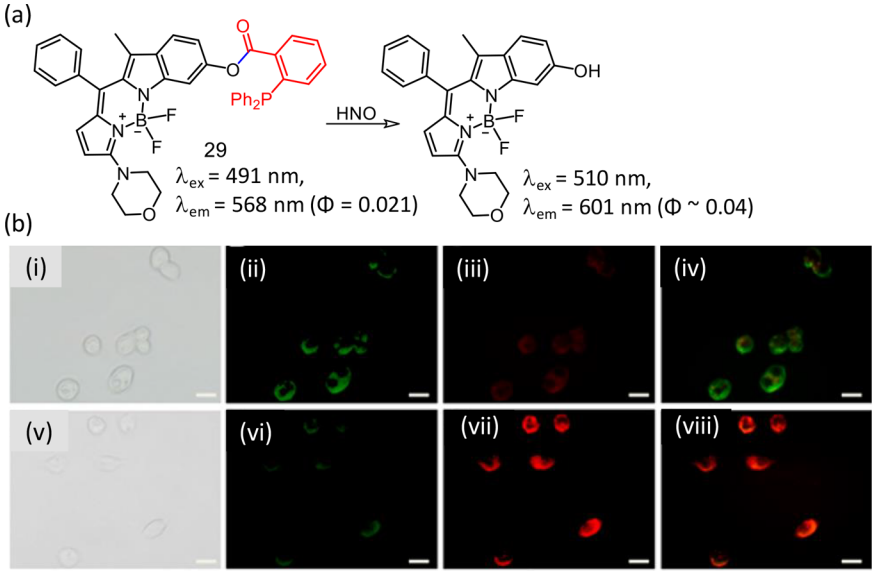

Figure 19. (a) Molecular structure of the reagent **29** and its reaction product, (b) CLSM images of HepG2 cells incubated with **29** (10 μM) for 30 min (i–v) and then with Angeli's salt (50 μM) for another 10 min (v–viii). (i, v) Bright-field imaging, (ii, vi) green window (510–550 nm), (iii, vii) red window (590–650 nm), and (iv, viii) ratio/merge image obtained from the red window to green window. Scale bar = 20 μm. Figure 19b was reprinted from ref 48. Copyright 2018, American Chemical Society.

https://dx.doi.org/10.1021/acsomega.9b03420
ACS Omega 2020, 5, 1730–1742

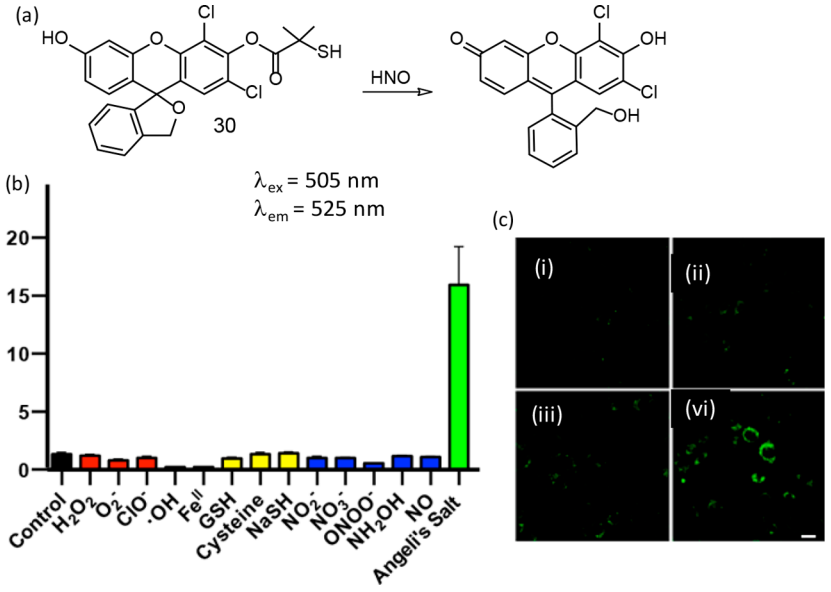

Figure 20. (a) Molecular structure of the reagent **30** and its reaction product, (b) response of the reagent **30** to various reactive oxygen, sulfur, and nitrogen species at concentrations of 100 μM (GSH was tested at 1 mM), (c) CLSM images of MDA-MB-231 cells treated with (i) 0 μM (vehicle control), (ii) 250 μM, (iii) 500 μM, and (iv) 1000 μM Angeli's salt for 15 min using a 488 nm laser source for excitation. Figure 20 (b and c) was reprinted from ref 49. Copyright 2017 American Chemical Society.

understanding the proper physiological function for HNO—which in turn would help us in designing appropriate and efficient receptors for HNO. The chemistry of HOCl is a little better understood. Still, there are many unanswered questions for the physiological role of HOCl, and the area of clinical diagnosis of endogenous HOCl still needs attention. Better insight into the HOCl defense mechanism at the molecular level and effective real-time quantification of endogenous HOCl would help not only in controlling many pathogenic bacteria by counteracting them but also for developing efficient molecular probes for HOCl.

AUTHOR INFORMATION

Corresponding Authors

Sumit Kumar Pramanik − *CSIR-Central Salt and Marine Chemicals Research Institute, Bhavnagar, India;* orcid.org/0000-0002-0294-8829; Email: sumitpramanik@csmcri.res.in

Amitava Das − *CSIR-Central Salt and Marine Chemicals Research Institute, Bhavnagar, India;* orcid.org/0000-0003-3666-1743; Email: a.das@csmcri.res.in

Other Authors

Anila Hoskere Ashoka − *Universitéde Strasbourg, Strasbourg, France*

Firoj Ali − *CSIR - Central Institute of Mining and Fuel Research, Dhanbad, India*

Rajeshwari Tiwari − *CSIR-Central Salt and Marine Chemicals Research Institute, Bhavnagar, India*

Rina Kumari − *CSIR-Central Salt and Marine Chemicals Research Institute, Bhavnagar, India*

Complete contact information is available at: https://pubs.acs.org/10.1021/acsomega.9b03420

Notes

The authors declare no competing financial interest.

Biographies

Anila Hoskere Ashoka pursued his research under the supervision of Dr. Amitava Das at CSIR-National Chemical Laboratory, and he was awarded a Ph.D. degree by AcSIR in 2018. Presently, Anila is a post-doctoral researcher at the Laboratory of Bioimaging and Pathologies, University of Strasbourg, France. His research interest centers around developing novel fluorescence probes and hybrid fluorescent materials for sensing and imaging applications.

Firoj Ali worked as a research scholar at the Organic Chemistry Division of CSIR-National Chemical Laboratory under the supervision of Dr. Amitava

https://dx.doi.org/10.1021/acsomega.9b03420
ACS Omega 2020, 5, 1730−1742

Das and obtained his Ph.D. in Chemistry from AcSIR in 2017. Before joining as a Scientist at Rock Excavation Engineering Division, CSIR-Central Institute of Mining and Fuel Research, Dhanbad, India in 2018, Firoj pursued his postdoctoral research at the School of Chemistry, University of Birmingham, UK. The primary aim of his research is to develop smart photoactive molecular probes for recognition of biomarkers and commercial explosives that are being used in the mining industry.

Rajeshwari Tiwari is an Inspire Fellow (DST, India) at CSIR-CSMCRI since 2018 and is pursuing her research for a Ph.D. degree under the joint supervision of Dr. Amitava Das and Dr. Sumit Kumar Pramanik of the Analytical Chemistry Division of CSIR-CSMCRI. Her area of interest is targeted drug delivery through nanocarriers.

Dr. Rina Kumari obtained her Ph.D. in 2016 from the Indian Institute of Technology Patna (India). She pursued her research for a Ph.D. degree at the Department of Chemistry under the mentorship of Professor Prolay Das. She then pursued her postdoctoral career as a SERB-National postdoctoral fellow at CSIR-CSMCRI, Bhavnagar, in the research group of Dr. Amitava Das. Her current research interests include nanotheranostics using self-assembled actively targeting biomolecule-based nanoclusters.

Sumit Kumar Pramanik is currently a Senior Scientist of CSIR-Central Salt and Marine Chemicals Research Institute, Bhavnagar. He earned his Bachelor's degree in Chemistry from Vidyasagar University and Masters in Applied Chemistry from Bengal Engineering and Science University, Shibpur. Afterward, he continued with graduate studies in Organic & Medicinal Chemistry at CSIR-Indian Institute of Chemical Biology, Kolkata, and obtained his doctoral degree in 2013. He was a postdoctoral fellow at Hasselt University (Belgium). His research interests are in the areas of analytical sensors for biological and point-of-care applications, synthesis of various functional materials and their application in therapeutics and diagnostics, and also the development of diagnostic/prognostic devices.

Amitava Das completed his basic education in Chemistry at Jadavpur University in Kolkata and continued to work there as a research scholar to pursue his research for a Ph.D. degree in Science in 1989. After availing the Nehru (Gov. of India)/SERC (UK) postdoctoral fellowship at Birmingham University/University of Bristol in the UK, he joined CSIR-CSMCRI in 1993. Amitava continued at CSIR-CSMCRI until 2013, when he moved as the Chief Scientist and Professor-AcSIR to CSIR-National Chemical Laboratory, Pune. He moved back to CSIR-CSMCRI in 2016 as the Director of the Institute and was Distinguished Professor of AcSIR. He is the elected fellow of all the three major academies of India, and he is also the recipient of the J. C. Bose National Fellowship since 2017. After superannuation from CSIR at the age of 60 years, he is expected to be associated with Indian Institutes of Science Education and Research Kolkata as a Professor in Chemical Sciences starting in January 2020. He is an Editorial Board Member of RSC Advances. His research interests focus on supramolecular chemistry, photoinduced processes, molecular recognition, biomarkers and bioimaging, and functional nanostructures.

■ ACKNOWLEDGMENTS

Financial support from SERB grants (EMR/2016/001850 and JCB/2017/000004) and a DBT (India) grant (BT/PR22251/NNT/28/1274/2017) is acknowledged by A.D. This manuscript bears CSMCRI registration number 6/2020.

■ REFERENCES

(1) Dickinson, B. C.; Chang, C. J. Chemistry and biology of reactive oxygen species in signaling or stress responses. *Nat. Chem. Biol.* **2011**, *7* (8), 504−511.

(2) Dharmaraja, A. T. Role of Reactive Oxygen Species (ROS) in Therapeutics and Drug Resistance in Cancer and Bacteria. *J. Med. Chem.* **2017**, *60* (8), 3221−3240.

(3) Singh, H.; Tiwari, K.; Tiwari, R.; Pramanik, S. K.; Das, A. Small Molecule as Fluorescent Probes for Monitoring Intracellular Enzymatic Transformations. *Chem. Rev.* **2019**, *119*, 11718.

https://dx.doi.org/10.1021/acsomega.9b03420
ACS Omega 2020, 5, 1730−1742

(4) Banerji, B.; Pramanik, S. K.; Sanphui, P.; Nikhar, S.; Biswas, S. C. Synthesis and Cytotoxicity Studies of Novel Triazolo-Benzoxazepine as New Anticancer Agents. *Chem. Biol. Drug Des.* **2013**, *82* (4), 401−409.
(5) Phaniendra, A.; Jestadi, D. B.; Periyasamy, L. Free radicals: properties, sources, targets, and their implication in various diseases. *Indian J. Clin. Biochem.* **2015**, *30* (1), 11−26.
(6) Di Meo, S.; Reed, T. T.; Venditti, P.; Victor, V. M. Role of ROS and RNS Sources in Physiological and Pathological Conditions. *Oxid. Med. Cell. Longevity* **2016**, *2016*, 1245049.
(7) Mittal, M.; Siddiqui, M. R.; Tran, K.; Reddy, S. P.; Malik, A. B. Reactive oxygen species in inflammation and tissue injury. *Antioxid. Redox Signaling* **2014**, *20* (7), 1126−1167.
(8) Nita, M.; Grzybowski, A. The Role of the Reactive Oxygen Species and Oxidative Stress in the Pathomechanism of the Age-Related Ocular Diseases and Other Pathologies of the Anterior and Posterior Eye Segments in Adults. *Oxid. Med. Cell. Longevity* **2016**, *2016*, 3164734.
(9) Lee, S. H.; Fujioka, S.; Takahashi, R.; Oe, T. Angiotensin II-Induced Oxidative Stress in Human Endothelial Cells: Modification of Cellular Molecules through Lipid Peroxidation. *Chem. Res. Toxicol.* **2019**, *32* (7), 1412−1422.
(10) Dupré-Crochet, S.; Erard, M.; Nüβe, O. ROS production in phagocytes: why, when, and where? *J. Leukocyte Biol.* **2013**, *94* (4), 657−670.
(11) Zhou, Z.; Song, J.; Nie, L.; Chen, X. Reactive oxygen species generating systems meeting challenges of photodynamic cancer therapy. *Chem. Soc. Rev.* **2016**, *45* (23), 6597−6626.
(12) Reisz, J. A.; Zink, C. N.; King, S. B. Rapid and selective nitroxyl (HNO) trapping by phosphines: kinetics and new aqueous ligations for HNO detection and quantitation. *J. Am. Chem. Soc.* **2011**, *133* (30), 11675−11685.
(13) Alluisetti, G. E.; Almaraz, A. E.; Amorebieta, V. T.; Doctorovich, F.; Olabe, J. A. Metal-Catalyzed Anaerobic Disproportionation of Hydroxylamine. Role of Diazene and Nitroxyl Intermediates in the Formation of N2, N2O, NO+, and NH3. *J. Am. Chem. Soc.* **2004**, *126* (41), 13432−13442.
(14) Ren, M.; Dong, B.; Lin, W. 10 - Fluorescent Probes for HNO Detection. In *The Chemistry and Biology of Nitroxyl (HNO)*; Doctorovich, F., Farmer, P. J., Marti, M. A., Eds.; Elsevier: Boston, 2017; pp 207−224.
(15) Ivanović-Burmazović, I. 5 - HNO Generation From NO, Nitrite, Inorganic or Organic Nitrosyls, and Crosstalk With H2S. In *The Chemistry and Biology of Nitroxyl (HNO)*; Doctorovich, F., Farmer, P. J., Marti, M. A., Eds.; Elsevier: Boston, 2017; pp 67−104.
(16) Basudhar, D.; Bharadwaj, G.; Salmon, D. J.; Miranda, K. M. 2 - HNO Donors: Angeli's Salt and Related Diazeniumdiolates. In *The Chemistry and Biology of Nitroxyl (HNO)*; Doctorovich, F., Farmer, P. J., Marti, M. A., Eds.; Elsevier: Boston, 2017; pp 11−36.
(17) Bartberger, M. D.; Fukuto, J. M.; Houk, K. N. On the acidity and reactivity of HNO in aqueous solution and biological systems. *Proc. Natl. Acad. Sci. U. S. A.* **2001**, *98* (5), 2194−2198.
(18) Shafirovich, V.; Lymar, S. V. Nitroxyl and its anion in aqueous solutions: Spin states, protic equilibria, and reactivities toward oxygen and nitric oxide. *Proc. Natl. Acad. Sci. U. S. A.* **2002**, *99* (11), 7340−7345.
(19) DeMaster, E. G.; Redfern, B.; Nagasawa, H. T. Mechanisms of Inhibition of Aldehyde Dehydrogenase by Nitroxyl, the Active Metabolite of the Alcohol Deterrent Agent Cyanamide. *Biochem. Pharmacol.* **1998**, *55* (12), 2007−2015.
(20) Zhang, W.; Guo, C.; Liu, L.; Qin, J.; Yang, C. Naked-eye visible and fluorometric dual-signaling chemodosimeter for hypochlorous acid based on water-soluble p-methoxyphenol derivative. *Org. Biomol. Chem.* **2011**, *9* (15), 5560−5563.
(21) Zhao, N.; Wu, Y.-H.; Wang, R.-M.; Shi, L.-X.; Chen, Z.-N. An iridium(iii) complex of oximated 2,2′-bipyridine as a sensitive phosphorescent sensor for hypochlorite. *Analyst* **2011**, *136* (11), 2277−2282.
(22) Lin, W.; Long, L.; Chen, B.; Tan, W. A Ratiometric Fluorescent Probe for Hypochlorite Based on a Deoximation Reaction. *Chem. - Eur. J.* **2009**, *15* (10), 2305−2309.
(23) Shi, J.; Li, Q.; Zhang, X.; Peng, M.; Qin, J.; Li, Z. Simple triphenylamine-based luminophore as a hypochlorite chemosensor. *Sens. Actuators, B* **2010**, *145* (1), 583−587.
(24) Cheng, X.; Jia, H.; Long, T.; Feng, J.; Qin, J.; Li, Z. A "turn-on" fluorescent probe for hypochlorous acid: convenient synthesis, good sensing performance, and a new design strategy by the removal of C−N isomerization. *Chem. Commun.* **2011**, *47* (43), 11978−11980.
(25) Zhou, Y.; Pei, W.; Wang, C.; Zhu, J.; Wu, J.; Yan, Q.; Huang, L.; Huang, W.; Yao, C.; Loo, J. S. C.; Zhang, Q. Rhodamine-Modified Upconversion Nanophosphors for Ratiometric Detection of Hypochlorous Acid in Aqueous Solution and Living Cells. *Small* **2014**, *10* (17), 3560−3567.
(26) Singh, H.; Sreedharan, S.; Tiwari, K.; Green, N. H.; Smythe, C.; Pramanik, S. K.; Thomas, J. A.; Das, A. Two photon excitable graphene quantum dots for structured illumination microscopy and imaging applications: lysosome specificity and tissue-dependent imaging. *Chem. Commun.* **2019**, *55* (4), 521−524.
(27) Pramanik, S. K.; Sreedharan, S.; Singh, H.; Green, N. H.; Smythe, C.; Thomas, J. A.; Das, A. Imaging cellular trafficking processes in real time using lysosome targeted up-conversion nanoparticles. *Chem. Commun.* **2017**, *53* (94), 12672−12675.
(28) Singh, H.; Sreedharan, S.; Tiwari, R.; Walther, C.; Smythe, C.; Pramanik, S. K.; Thomas, J. A.; Das, A. A Fluorescent Chemodosimeter for Organelle-Specific Imaging of Nucleoside Polyphosphate Dynamics in Living Cells. *Cryst. Growth Des.* **2018**, *18* (11), 7199−7206.
(29) Zhan, X.-Q.; Yan, J.-H.; Su, J.-H.; Wang, Y.-C.; He, J.; Wang, S.-Y.; Zheng, H.; Xu, J.-G. Thiospirolactone as a recognition site: Rhodamine B-based fluorescent probe for imaging hypochlorous acid generated in human neutrophil cells. *Sens. Actuators, B* **2010**, *150* (2), 774−780.
(30) Kenmoku, S.; Urano, Y.; Kojima, H.; Nagano, T. Development of a Highly Specific Rhodamine-Based Fluorescence Probe for Hypochlorous Acid and Its Application to Real-Time Imaging of Phagocytosis. *J. Am. Chem. Soc.* **2007**, *129* (23), 7313−7318.
(31) Liu, C.; Li, Z.; Yu, C.; Chen, Y.; Liu, D.; Zhuang, Z.; Jia, P.; Zhu, H.; Zhang, X.; Yu, Y.; Zhu, B.; Sheng, W. Development of a Concise Rhodamine-Formylhydrazine Type Fluorescent Probe for Highly Specific and Ultrasensitive Tracing of Basal HOCl in Live Cells and Zebrafish. *ACS Sensors* **2019**, *4* (8), 2156−2163.
(32) Wu, L.; Wu, I. C.; DuFort, C. C.; Carlson, M. A.; Wu, X.; Chen, L.; Kuo, C.-T.; Qin, Y.; Yu, J.; Hingorani, S. R.; Chiu, D. T. Photostable Ratiometric Pdot Probe for in Vitro and in Vivo Imaging of Hypochlorous Acid. *J. Am. Chem. Soc.* **2017**, *139* (20), 6911−6918.
(33) Liu, Z.; Gao, K.; Wang, B.; Yan, H.; Xing, P.; Zhong, C.; Xu, Y.; Li, H.; Chen, J.; Wang, W.; Sun, S. A dinuclear ruthenium(II) complex as turn-on luminescent probe for hypochlorous acid and its application for in vivo imaging. *Sci. Rep.* **2016**, *6*, 29065.
(34) Ali, F.; Aute, S.; Sreedharan, S.; Anila, H. A.; Saeed, H. K.; Smythe, C. G.; Thomas, J. A.; Das, A. Tracking HOCl concentrations across cellular organelles in real time using a super resolution microscopy probe. *Chem. Commun.* **2018**, *54* (15), 1849−1852.
(35) Yuan, L.; Wang, L.; Agrawalla, B. K.; Park, S.-J.; Zhu, H.; Sivaraman, B.; Peng, J.; Xu, Q.-H.; Chang, Y.-T. Development of Targetable Two-Photon Fluorescent Probes to Image Hypochlorous Acid in Mitochondria and Lysosome in Live Cell and Inflamed Mouse Model. *J. Am. Chem. Soc.* **2015**, *137* (18), 5930−5938.
(36) Xu, Q.; Heo, C. H.; Kim, J. A.; Lee, H. S.; Hu, Y.; Kim, D.; Swamy, K. M. K.; Kim, G.; Nam, S.-J.; Kim, H. M.; Yoon, J. A Selective Imidazoline-2-thione-Bearing Two-Photon Fluorescent Probe for Hypochlorous Acid in Mitochondria. *Anal. Chem.* **2016**, *88* (12), 6615−6620.
(37) Zhang, B.; Yang, X.; Zhang, R.; Liu, Y.; Ren, X.; Xian, M.; Ye, Y.; Zhao, Y. Lysosomal-Targeted Two-Photon Fluorescent Probe to Sense Hypochlorous Acid in Live Cells. *Anal. Chem.* **2017**, *89* (19), 10384−10390.
(38) Pak, Y. L.; Park, S. J.; Song, G.; Yim, Y.; Kang, H.; Kim, H. M.; Bouffard, J.; Yoon, J. Endoplasmic Reticulum-Targeted Ratiometric N-Heterocyclic Carbene Borane Probe for Two-Photon Microscopic

https://dx.doi.org/10.1021/acsomega.9b03420
ACS Omega 2020, 5, 1730−1742

Imaging of Hypochlorous Acid. *Anal. Chem.* **2018**, *90* (21), 12937−12943.
(39) Shi, D.; Chen, S.; Dong, B.; Zhang, Y.; Sheng, C.; James, T. D.; Guo, Y. Evaluation of HOCl-generating anticancer agents by an ultrasensitive dual-mode fluorescent probe. *Chem. Sci.* **2019**, *10* (13), 3715−3722.
(40) Fukuto, J. M. A recent history of nitroxyl chemistry, pharmacology and therapeutic potential. *Br. J. Pharmacol.* **2019**, *176* (2), 135−146.
(41) Apfel, U.-P.; Buccella, D.; Wilson, J. J.; Lippard, S. J. Detection of Nitric Oxide and Nitroxyl with Benzoresorufin-Based Fluorescent Sensors. *Inorg. Chem.* **2013**, *52* (6), 3285−3294.
(42) Wrobel, A. T.; Johnstone, T. C.; Deliz Liang, A.; Lippard, S. J.; Rivera-Fuentes, P. A Fast and Selective Near-Infrared Fluorescent Sensor for Multicolor Imaging of Biological Nitroxyl (HNO). *J. Am. Chem. Soc.* **2014**, *136* (12), 4697−4705.
(43) Kim, S.; Minier, M. A.; Loas, A.; Becker, S.; Wang, F.; Lippard, S. J. Achieving Reversible Sensing of Nitroxyl by Tuning the Ligand Environment of Azamacrocyclic Copper(II) Complexes. *J. Am. Chem. Soc.* **2016**, *138* (6), 1804−1807.
(44) Kawai, K.; Ieda, N.; Aizawa, K.; Suzuki, T.; Miyata, N.; Nakagawa, H. A Reductant-Resistant and Metal-Free Fluorescent Probe for Nitroxyl Applicable to Living Cells. *J. Am. Chem. Soc.* **2013**, *135* (34), 12690−12696.
(45) Dong, B.; Zheng, K.; Tang, Y.; Lin, W. Development of green to near-infrared turn-on fluorescent probes for the multicolour imaging of nitroxyl in living systems. *J. Mater. Chem. B* **2016**, *4* (7), 1263−1269.
(46) Dong, B.; Song, X.; Kong, X.; Wang, C.; Zhang, N.; Lin, W. Two-photon red-emissive fluorescent probe for imaging nitroxyl (HNO) in living cells and tissues. *J. Mater. Chem. B* **2017**, *5* (26), 5218−5224.
(47) Ali, F.; Sreedharan, S.; Ashoka, A. H.; Saeed, H. K.; Smythe, C. G. W.; Thomas, J. A.; Das, A. A Super-Resolution Probe To Monitor HNO Levels in the Endoplasmic Reticulum of Cells. *Anal. Chem.* **2017**, *89* (22), 12087−12093.
(48) Yuan, S.; Wang, F.; Yang, G.; Lu, C.; Nie, J.; Chen, Z.; Ren, J.; Qiu, Y.; Sun, Q.; Zhao, C.; Zhu, W.-H. Highly Sensitive Ratiometric Self-Assembled Micellar Nanoprobe for Nitroxyl and Its Application In Vivo. *Anal. Chem.* **2018**, *90* (6), 3914−3919.
(49) Pino, N. W.; Davis, J.; Yu, Z.; Chan, J. Nitroxyl Fluor: A Thiol-Based Fluorescent Probe for Live-Cell Imaging of Nitroxyl. *J. Am. Chem. Soc.* **2017**, *139* (51), 18476−18479.

https://dx.doi.org/10.1021/acsomega.9b03420
ACS Omega 2020, 5, 1730−1742